

Thin Film Evaporative Cooling in Microgap Channels

A. Bar-Cohen, J. Sheehan, A. Elbaz, C. Holloway

*University of Maryland, Department of Mechanical Engineering, TherPES Laboratory
2106B Glenn Martin Hall, College Park, MD 20742, US*

Tel: 301-405-3173; abc@umd.edu

ABSTRACT

Evaporation of dielectric coolants and refrigerants flowing in microgap channels and tubes, is a most promising - though as yet insufficiently understood - technique for a wide range of energy conversion applications and of particular interest in the thermal management of high flux semiconductor chips, chip stacks, and other microelectronic components. In such microgap channels, Annular flow has been found to be the dominant flow regime and to provide substantial evaporative heat transfer rates at the wetted walls. This Keynote lecture will review two-phase flow regimes in microgap channels and the M-shaped heat transfer coefficient variation induced by the axial progression from Bubble to Annular flow. Attention will then be turned to the observed spatial and temporal variations in the wetted wall temperature and to the articulation of an inverse technique for extracting local heat transfer coefficients from such data. Recent results for the parametric dependence of the wall temperature fluctuations and zonal heat transfer coefficients, as well as the impact of microgap channel orientation and externally imposed vibrations on wall temperature, will be described.

Keywords: evaporation; two-phase flow; boiling; microgaps, microchannels

INTRODUCTION

The Moore's law progression in semiconductor technology, including shrinking feature size, increasing transistor density, and faster circuit speeds, as well as the introduction of new nitride-based materials for Power Amplifiers (PA), RF, and telecommunication applications, is leading to ever higher chip power dissipation and heat fluxes. Roadmap projections suggest that the maximum microprocessor chip power dissipation will exceed 500W and heat flux exceed $150\text{W}/\text{cm}^2$ within the next few years. The thermal management challenge is further exacerbated by the appearance of localized, sub-millimeter hot spots, often exceeding $1\text{kW}/\text{cm}^2$ in heat flux, in microprocessor, MMIC, PA, and IGBT chips, which can degrade performance and reliability. Among the aggressive techniques which can be applied to such high performance electronic systems, microgap coolers – relying on the evaporation of dielectric liquids circulating in the narrow gaps inherent in compact packaging structures or microchannels created in chips and substrates – could provide unique advantages. Microgap coolers, unlike many current thermal management devices, eliminate the high and problematic thermal contact resistance associated with coldplates and heat sinks by allowing heat flow directly from the dissipative components into the dielectric liquid. While the value of the heat transfer coefficients that develop in such microgap channels is not yet precisely predictable, it is clear that evaporation and two-phase flow of dielectric fluids can produce heat transfer coefficients comparable to forced convection with water. Due to the elimination of distinct heat exchangers or cold plates, microgap coolers can also provide significant weight, cost, and volume benefits relative to competing cooling technologies. Additionally, microgap coolers can be used to cool individual components and/or an interposer in a chip stack, providing a promising solution for these emerging packaging challenges.

CONFINED TWO-PHASE FLOW

The simultaneous flow of vapor and liquid in a confined channel or tube can take various forms depending on the distribution and extent of aggregation of the two phases, with each distinct vapor/liquid distribution referred to as a “flow regime.” Four primary two-phase flow regimes: Bubble, Intermittent, Annular, and Stratified, as well as numerous sub-regimes, have been identified in the literature, e.g. Hetsroni (1982). Bubble flow is associated with a uniform distribution of

small spherical bubbles moving in tandem within the liquid phase. Intermittent flow is characterized by the flow of liquid plugs separated by elongated gas bubbles – often in the shape of slugs or bullets – though sometimes more chaotically mixed. In Annular flow, a relatively thin liquid layer flows along the channel walls, while the vapor flows in the center of the channel, creating a vapor “core” which may also contain entrained droplets. In vertical channels with heat addition, where the vapor content increases in the flow direction, the Bubble regime is followed sequentially by the Intermittent and Annular regimes. In horizontal or near-horizontal, channels – in addition to the three regimes encountered in vertical channels – two phase flow may also occur in a Stratified pattern in which the liquid flows along the lower surface and the vapor above. This Stratified flow pattern generally occurs at relatively low liquid and vapor flow rates and, as the flow rates increase, transitions into Intermittent or Annular flow, as shown in Figure 1.

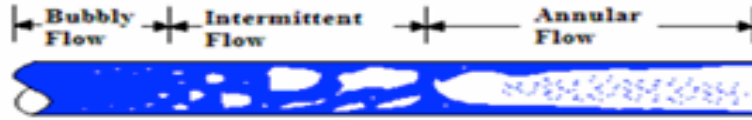


Figure 1: Two-Phase Flow in a Uniformly Heated Horizontal Pipe, Bar-Cohen et al (2009).

An appreciation for the dependence of thermo-fluid parameters on the form, as well as extent, of aggregation of each phase, led early researchers to describe and map the gas-liquid and vapor-liquid flow regimes prevailing in channels used to generate and/or transport two-phase flows [Baker (1954), Mandhane et al. (1974), Taitel and Dukler (1976), and Weisman et al. (1979)]. Most noteworthy among these was the pioneering effort by Taitel and Dukler, defining and mapping the four predominant flow regimes (Stratified, Intermittent, Bubble, and Annular) with superficial gas and superficial liquid coordinates and proposing physics-based criteria for the transition from one regime to the next. After considerable additional contributions by Barnea et al (1980), Shoham (1982), and Taitel and Dukler (1987), in 1990 this effort culminated in the Unified Model for predicting flow regime transitions in channels of any orientation, based on simple physical criteria and using familiar two-phase non-dimensional groupings.

Figure 2 displays such a map, using the Froude number (Eq. 1), the T parameter (relating the liquid pressure drop to buoyancy, as in Eq. 2 below), and the Martinelli number (Eq. 3) with the superimposed locus traced out by the data of Yang and Fujita (2004) for R113 flowing in micro gap channels, with the gap size ranging from 0.2 mm to 2 mm.

$$F = \sqrt{\frac{\rho_G}{\rho_L - \rho_G}} \frac{U_{SG}}{D g \cos \beta} \quad (1)$$

$$T = \left[\frac{\left[\frac{dP}{dx} \right]_{SL}}{(\rho_L - \rho_G) g \cos \beta} \right]^{1/2} \quad (2)$$

$$X = \left[\frac{\left[\frac{dP}{dx} \right]_{SL}}{\left[\frac{dP}{dx} \right]_{SG}} \right]^{1/2} \quad (3)$$

It is to be noted that the specific formulations used in developing the regime transition criteria reflect the distinction between surface tension driven regimes, such as Bubble and Intermittent flow, and shear force driven regimes, such as Stratified and Annular flow. The models contain little empiricism, and, therefore, can be applied to most fluids and be extrapolated to conditions other than water-air and water-steam flowing in the 25 mm and larger pipes that were used in the original experimental verification of the approach, Shoham (1982), Taitel and Dukler (1987).

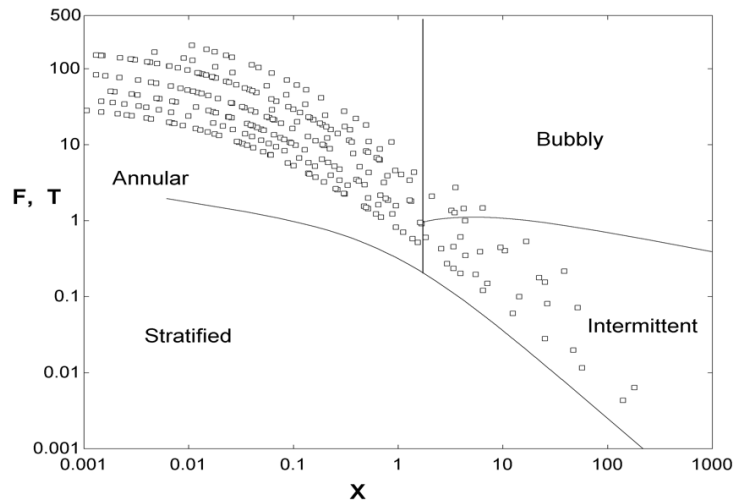


Figure 2: Taitel-Dukler Non-dimensional Two-Phase Flow Regime Map for Horizontal Microgap Channel (data of Yang and Fujita (2004): 0.2 – 2 mm gap, R113, $G = 50 - 200 \text{ kg/m}^2\text{s}$, $q = 20 - 90 \text{ kW/m}^2$, Rahim et al (2010)).

In embracing the use of this flow regime map, it must, nevertheless, be recognized that the Taitel-Dukler methodology relies on adiabatic models that ignore the thermal interactions between phases, the pipe, and the environment all of which are present in diabatic systems, in which heat is added or extracted from the flowing two-phase mixture. Nevertheless, the model has proven to be exceedingly useful for diabatic conditions and has demonstrated its first-order accuracy in numerous studies, including those performed by Taitel and Dukler (1978), Frankum et al. (1997), and Bar-Cohen and Rahim (2009). Although the non-dimensional maps provide a compact way to represent specific transitions, for ease of interpretation and a more physical representation of the flow regime distribution, it is convenient to use the dimensional form of the Taitel-Dukler flow regime map, with superficial velocity coordinates, as shown in Figure 3.

Recent studies of two-phase flow in miniature channels, including Harirchian and Garimella (2008), Megahed and Hassan (2009), and Bar-Cohen and Rahim (2009) have affirmed the existence of the three primary flow regimes, along with Stratified flow for horizontal configurations, in miniature channels, with Annular flow dominating in the smallest channels and Bubble flow, most common in channels with larger diameters and low quality flow. More recently, Rahim et al (2010) applied the Taitel-Dukler mapping methodology to the full Revellin et al (2005) dataset of flow regime observations for R134a and R245fa, flowing through 30-70mm long, 0.509 mm and 0.790 mm diameter glass channels, at pressures ranging from 665 kPa to 887 kPa for R134a and at 213kPa for R245fa. Their analysis revealed that 67% of the 2239 empirically observed flow pattern data points and 92% of the Annular flow data, was in the theoretically predicted regime, as shown for selected data in Figure 3. The authors also noted that further improvements in the flow regime predictions could be obtain by applying physics-based refinements to these transition criteria.

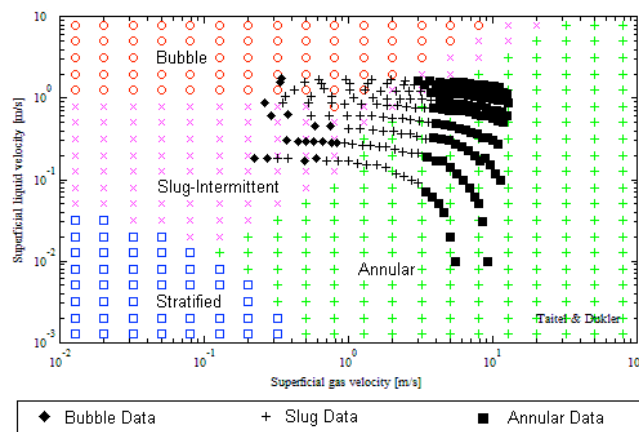


Figure 3: Taitel-Dukler flow regime map for data of R134a in 790 micron channel. $T_{\text{sat}} = 30^\circ\text{C}$, $T_{\text{Inlet-sub}} = 3 \text{ K}$, $G = 200 - 2000 \text{ kg/m}^2\text{s}$, Rahim et al (2010).

Analysis of available miniature channel two-phase data, including Lee et al (2001), Yang et al (2004), Kuznetsov and Shamirzaev (2006), as well as studies by Harirchian and Garimella (2008) and Mikielewicz et al (2012), have revealed a characteristic M-shaped variation of the heat transfer coefficient, as shown in 4. The inflection points in this M-shaped curve were found to equate approximately with flow regime transitions, including a first maximum at the transition from Bubble to Intermittent flow, a decreasing heat transfer coefficient in the Intermittent regime, followed by an increase on transition to Annular flow, and a second maximum, at relatively high qualities, that was suggested to result from the initiation of local dryout on the heated wall (Bar-Cohen and Rahim, 2009).

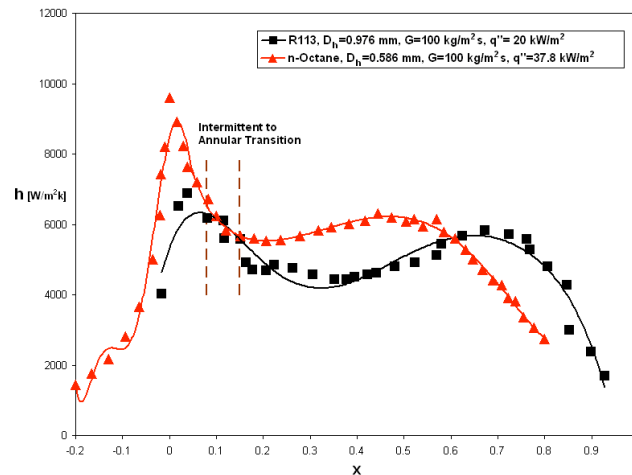


Figure 4: Two-phase flow characteristic M-shaped variation of the heat transfer coefficient, Bar-Cohen and Rahim (2009).

EXPERIMENTAL METHODOLOGY

Experimental Apparatus:

To aid in understanding the two-phase behavior of microgap channels and, in particular, to explore the circumstances surrounding the second maximum in the M-shaped heat transfer coefficient curve, a sequence of microgap channel experiments was initiated.

Figure 5 shows a digital image of the 1cm wide by 3cm long microgap channel, with height varying from 100 μ m to 500 μ m. Dielectric liquid was used as the working fluid and the asymmetrically-heated microgap channel wall was instrumented with thermocouples and pressure transducers, as described in Sheehan and Bar-Cohen (2009). A translucent sapphire viewing window, fitted into the Plexiglas top plate, was provided opposite the heated wall to facilitate Infrared thermography of the wall. A FLIR Merlin infrared camera was used for all experimentation at 60 Hz frame rate with an accuracy of $\pm 1^\circ\text{C}$.

Embedded thermocouples, located 1 mm below the imaged surface, were used to calibrate the infrared images, by matching the average infrared temperature to that of the thermocouples. Ceramic leaded chip resistors, 1cm x 1cm, were soldered directly to the bottom of the copper base plate and used to generate an average heat flux of up to 60W/cm². When cooled at a mass flux between 195 kg/m²-s and 780 kg/m²-s, the experimental microgap channel was found to operate partially in Intermittent and largely in Annular flow.

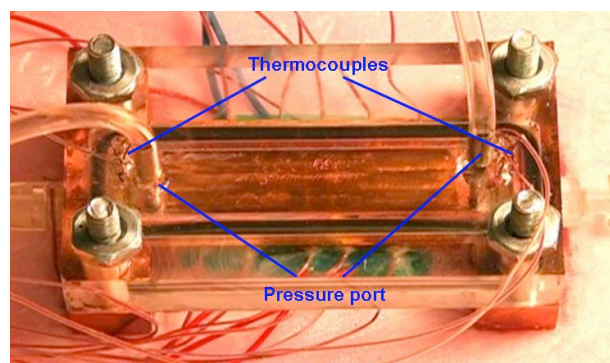


Figure 5: Photograph of 35 mm x 10 mm x 210 μ m microgap cooler, Kim (2007).

Inverse Computation:

In the absence of measured heat fluxes, an IR-based, inverse computation, with a detailed Finite-Element (ANSYS) model was used to determine the local microgap channel heat transfer coefficients responsible for the observed temperature profile. Typically, some 20 iterations of the assumed heat transfer coefficients, at the 8 thermocouple locations, were needed to achieve agreement to within 1K (or better) between the experimental and numerical temperature profile. Typical results of this inverse procedure are shown in Figure 6 and served as the basis for the determination of the zonal heat transfer coefficients.

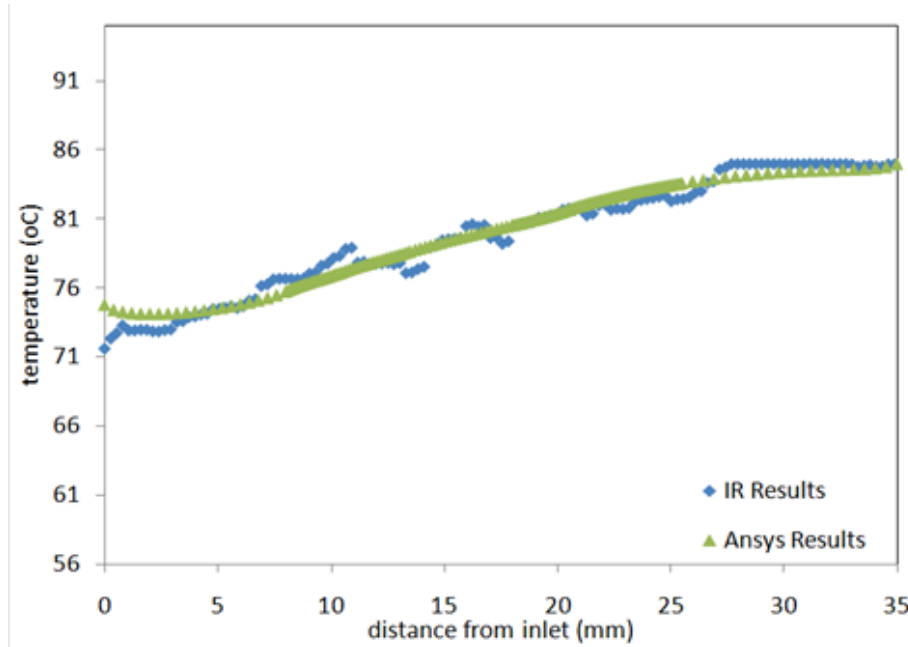


Figure 6: Experimental and Inversely Determined Numerical Axial Microgap Wall Temperature Distribution for FC-72 – 210 μm gap; $G = 195 \text{ kg/m}^2\text{-s}$; $q'' = 31 \text{ W/cm}^2$.

EMPERICAL WALL TEMPERATURE VARIATIONS

Figure 7 shows a sequence of four IR images taken 1second apart through the sapphire window in the microgap channel. The temperature non-uniformity and the high frequency of temperature fluctuations, in what might have been expected to be a quiescent regime of thin film evaporation, are clearly visible in these images.

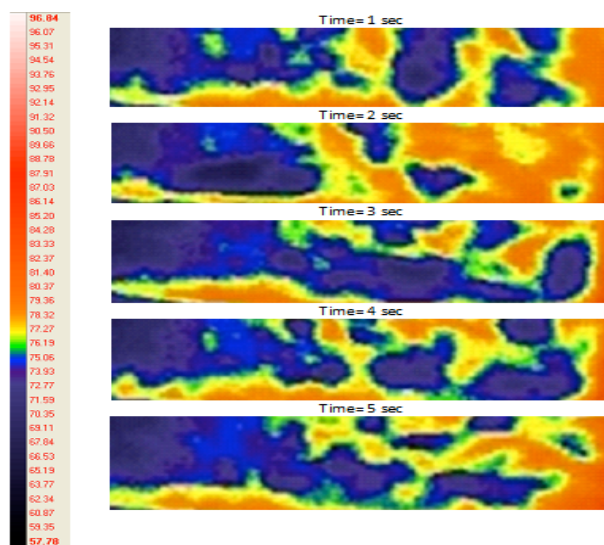


Figure 7: Sequential IR Thermography for FC-72 Flowing in 37 mm x 10 mm x 210 μm Microgap Channel – $G = 195.2 \text{ kg/m}^2\text{s}$, and $q'' = 22 \text{ W/cm}^2$, 4 images – 1 sec apart.

Figure 8 shows the instantaneous axial temperature variation from the inlet to the outlet of the 35mm microgap channel, for four different heat fluxes, taken along the center line of the channel. It is to be noted that in this “snapshot” the wall temperatures at all four fluxes increase from the inlet to the outlet, though more strongly with the highest heat flux, accompanied by modest spatial temperature fluctuations. Since the thermodynamic quality of the two-phase mixture depends on the total heat addition to the flow, the quality at each location varies with the surface heat flux, reaching dryout for the highest heat flux of $26\text{W}/\text{cm}^2$ and just 40% quality for $q'' = 10.3\text{W}/\text{cm}^2$, for the stated conditions. Figure 8 also reveals that, as expected, the wall temperatures for the highest heat flux are significantly higher than for the lowest heat flux. However, due to the dynamics of liquid film thinning with quality, the wall temperatures for the two middle heat fluxes converge to each other. Despite modest axial temperature variations, preliminary data for a higher heat flux shows a distinct difference between temperature fluctuations at two axial locations, as seen in Figure 9. This shows that a 9 mm separation can result in a 16K difference in fluctuation amplitude.

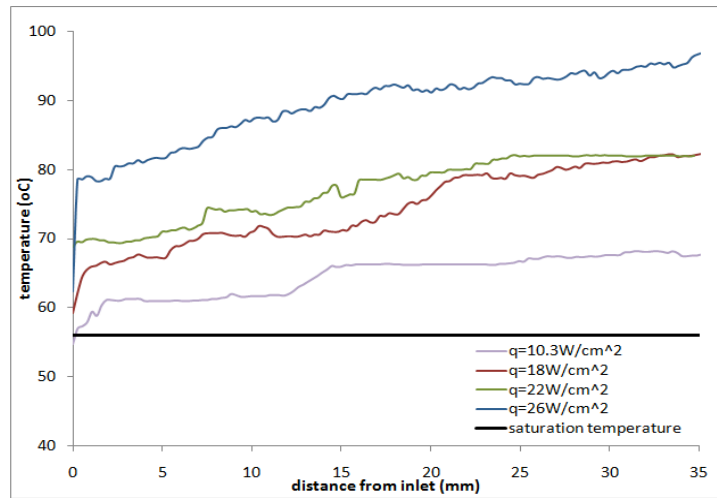


Figure 8: Axial Temperature Variation in 210 micron Microgap Cooler with $G = 195.2 \text{ kg}/\text{m}^2\text{-s}$ with FC-72 Working Fluid, Sheehan and Bar-Cohen (2010).

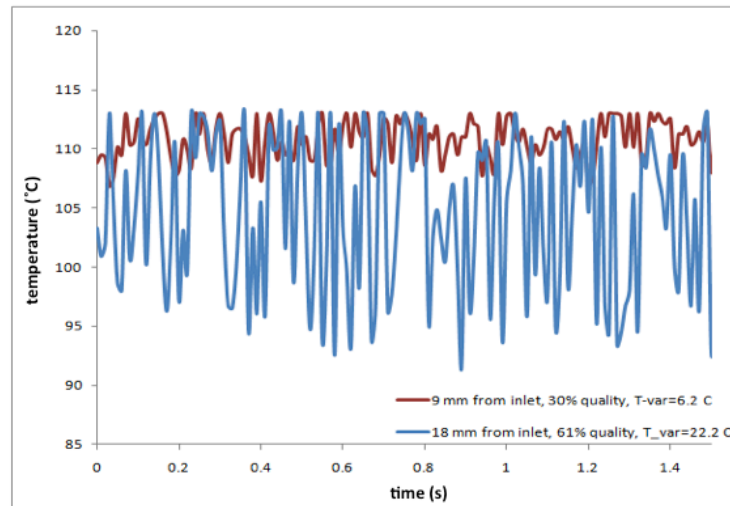


Figure 9: Comparison of two fixed locations within a 210 micron microgap cooler using FC-72 with $G = 195.2 \text{ kg}/\text{m}^2\text{-s}$ and $q = 30 \text{ W}/\text{cm}^2$, Sheehan and Bar-Cohen (2010).

Figure 10 displays the temporal temperature fluctuations at the 20mm downstream, location in the 210micron microgap channel, operating with a mass flux of $G=195.2 \text{ kg/m}^2\text{-s}$ and a range of heat fluxes. It is notable that high amplitude fluctuations occur at $q''=26\text{W/cm}^2$ and a quality of 0.56, while very modest fluctuations are encountered at a heat flux of 10.3W/cm^2 and a quality of 0.12. These variations are largely attributable to the changes in flow regime with quality but, in the prevailing Annular flow regime, appear to reflect the contribution, as well, of the heat flux to variations in the local film thickness.

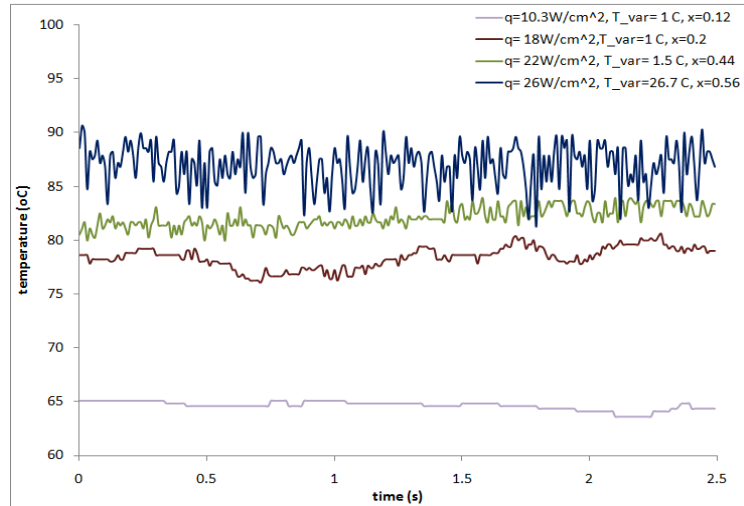


Figure 10: Temporal Temperature Variations at 20 mm Downstream Location - for a 210 micron channel with $G = 195.2 \text{ kg/m}^2\text{-s}$, Sheehan and Bar-Cohen (2010).

LOCAL MICROGAP HEAT TRANSFER COEFFICIENTS

In a parallel study (Rahim et al 2012), using Intel’s 11mm x 14mm Thermal Test Vehicle to simulate an actual silicon die, local heat transfer coefficients were obtained via the inverse calculation procedure described above and compared to the predictions of two classical correlations by Chen and Shah. As can be seen in Table 1, the average discrepancy between local h ’s and the Chen correlation for Annular flow is approximately 23% and results for Intermittent flow can be predicted to within 33% by both correlations. The agreement between data and correlations shows some dependence on gap size, with the larger gap of 500 micron showing 20% agreement with Chen and deteriorating as the gap size get smaller to 54% for the 100 micron channel. The discrepancy was moderately smaller for FC-87 data than HFE-7100 data, with the FC-87 data showing discrepancy of 26% and 41% with Chen and Shah, respectively, while the HFE-7100 data was found to show a discrepancy of 35% and 53% with same correlations.

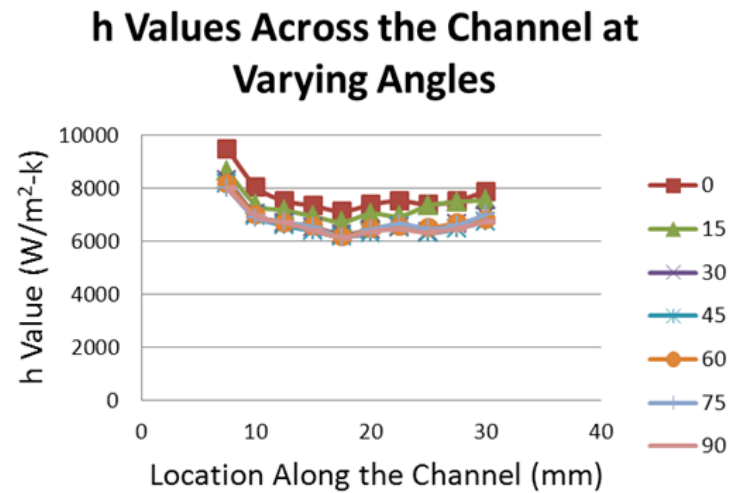
Table 1: Predicted and Inverse Calculated Local Heat Transfer Coefficients, Rahim et al, (2012).

Local Heat Transfer Coefficients Comparison		Number of Points	Discrepancy %	
			Chen	Shah
All Data		6210	30	47
Fluid	HFE-7100	3096	35	53
	FC-87	3114	26	41
Gap Size (micron)	100	1404	54	85
	200	1926	28	52
	500	2880	20	25
Flow Regime	Intermittent	4338	33	33
	Annular	1872	23	78

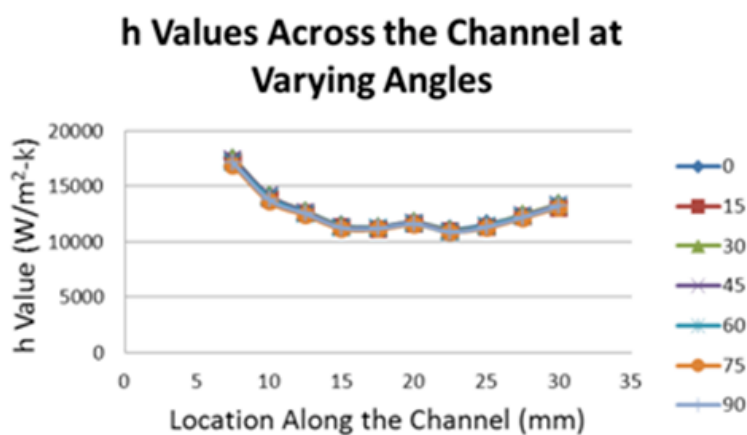
OPERATIONAL MICROGAP EFFECTS

Under operational conditions, electronic modules may be subjected to orientation changes and may experience substantial random vibration from the underlying structure or from other equipment nearby. In Figure 11 the sensitivity of the local microgap heat transfer coefficient to a change in orientation, from horizontal to vertical, is displayed for FC-72 flowing in a 210 micron high channel at two different mass fluxes and heat fluxes. In Fig 11a, it may be seen that at the low mass flux of $195\text{kg/m}^2\text{-s}$ and a heat flux of 24W/cm^2 , the horizontal orientation yields approximately 15% higher microgap heat transfer coefficients, consistently along the channel. However, at an increased mass flux of $488\text{kg/m}^2\text{-s}$, even in the presence of a 60W/cm^2 heat flux, there are no statistically significant variations of the local heat transfer coefficients with orientation.

The effect of simultaneous, three-axis vibrational excitation, representative of that experienced by a wheeled vehicle, on two-phase heat transfer in a microgap channel was studied by subjecting a 35mm long, 200 micron high channel to the Mil Standard 810F vibrational profile for wheeled vehicles. The spectral distribution of the forcing function and the axial temperature distribution for a 22.5W/cm^2 wall heat flux in the microgap channel are shown in Figure 12a and 12b, respectively. It may be seen that for a $500\text{kg/m}^2\text{-s}$ mass flux of HFE7100 in the 35mm long microgap channel, typifying results obtained with a broad range of heat fluxes for Intermittent and Annular flow, the wall temperature is nearly unaffected by the imposed vibration, experiencing less than 0.5K decrease relative to the quiescent condition.



(a)



(b)

Figure 11: Variation of Local Heat Transfer Coefficients with Orientation for FC72 Flowing in a $210\mu\text{m}$ Microgap Channel: (a) $q'' = 24\text{ W/cm}^2$ and $G = 195\text{ kg/m}^2\text{-s}$; (b) $q'' = 60\text{ W/cm}^2$ & $G = 488\text{ kg/m}^2\text{-s}$.

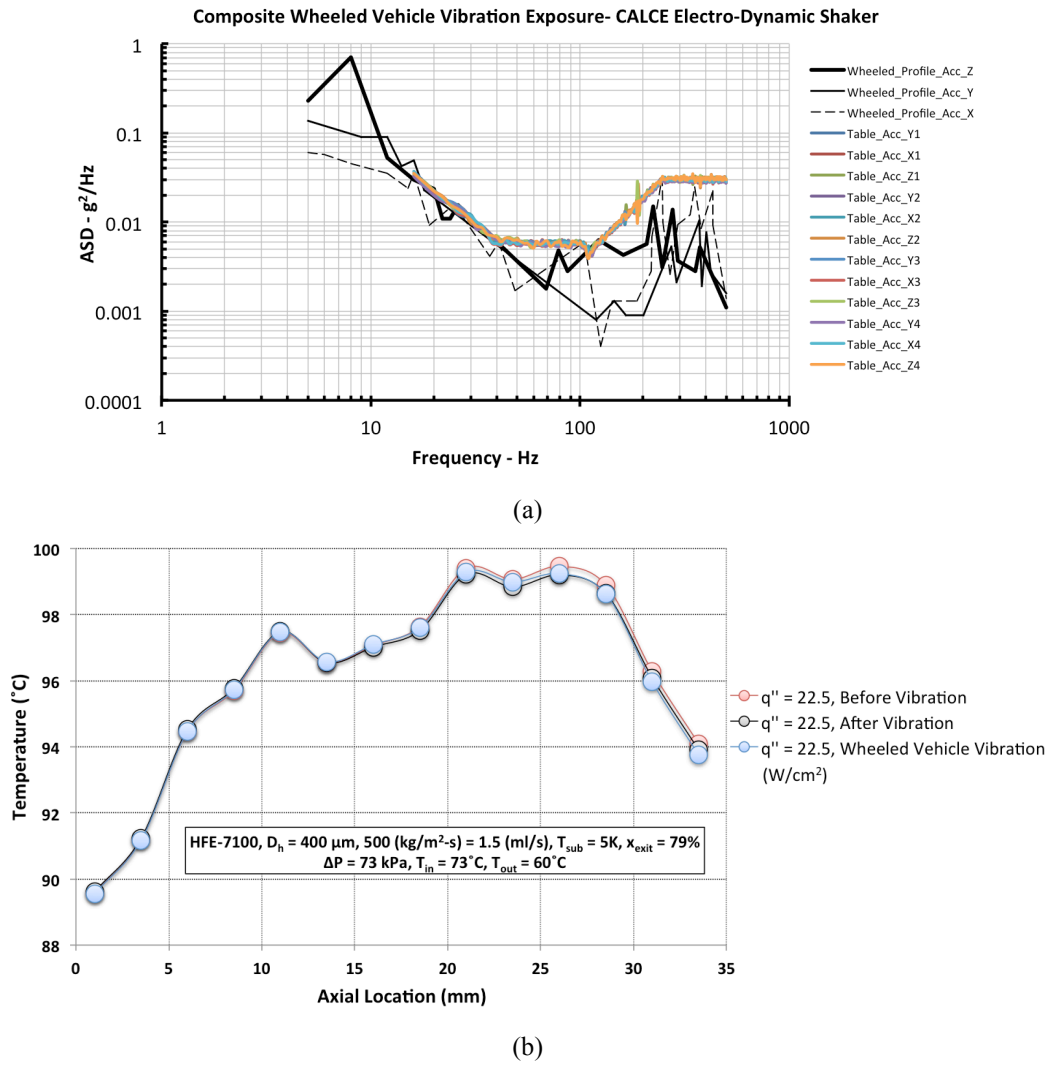


Figure 12: Random Vibrational Effects on Temperature Distribution in Two-Phase Microgap Channel with 200 μ m Gap: (a) MIL-STD-810F Random Vibration PSD profiles - Composite Wheeled Vehicle; (b) Axial Temperature Distribution.

Acknowledgments

The study described was supported by the Office of Naval Research and the L-3 Corporation. The authors wish to also thank 3M for providing the FC-72 used in these experiments.

References

- Baker, O., 1954, Simultaneous Flow of Oil and Gas, *Oil and Gas Journal*, Vol. 53, no. 12, pp. 185-195.
- Bar-Cohen, A., Ruder, Z., and Griffith, P., 1987, Thermal and Hydrodynamic Phenomena in a Horizontal Uniformly Heated Steam Generating Pipe, *Journal of Heat Transfer*, Vol. 109, no. 3, pp. 739-745.
- Bar-Cohen, A. and E. Rahim, 2009, Modeling and Prediction of Two-Phase Refrigerant Flow Regimes and Heat Transfer Characteristics in Microgap Channel, *Heat Transfer Engineering*, 30 (8), 601 – 625.
- Barnea, D., Unified Model for Predicting Flow-Pattern Transitions for the Whole Range of Pipe Inclinations, 1987, *International Journal of Multiphase Flow*, Vol. 8, no. 3, pp. 243-253.
- Bennett, D.L., and Chen, J.C., 1980, Forced convective boiling in vertical tubes for saturated pure components and binary mixtures, *AIChE Journal*, vol. 26, pp. 454 – 461.
- Chen, J.C., 1966, Correlation for boiling heat transfer to saturated fluids in convective flow, *Industrial and Engineering Chemistry - Process Design and Development*, Vol. 5 no. 3, pp. 322-329.
- Collier J.G., 1981, Forced Convective Boiling, in *Two-Phase Flow and Heat Transfer in the Power and Process Industries*, eds. A. E. Bergles, J. G. Collier, J. M. Delhaye, G. F. Hewitt, and F. Mayinger, Hemisphere, New York, NY.
- Dittus, F.W. and Boelter, L.M.K., 1930, Heat transfer in automobile radiators of the tubular type. *University of California Publications in Engineering*, vol. 2, pp. 443 – 461.
- Forster, H.K., and Zuber, N., 1955, Dynamics of vapor bubbles and boiling heat transfer, *AIChE, Journal*, vol. 1, no. 4, pp. 531 – 535.
- Frankum, D.P., Wadekar, V.V., and Azzopardi, B.J., 1997, Two-Phase Flow Patterns for Evaporating Flow, *Experimental Thermal and Fluid Science*, Vol. 15, no. 3, 183-192.
- Harirchian, T., and Garimella, S., 2008. An Investigation of Flow Boiling Regimes in Microchannels of Different Sizes by Means of High-Speed Visualization , *Proceedings of ITherm 2008*, Orlando, FL, USA.
- Hewitt, G.F., Liquid-Gas Systems, 1982, Flow Regimes, in *Handbook of Multiphase Systems*, ed. G. Hetsroni, pp. 2-3 – 2-43, Hemisphere, Washington, D.C.
- Kim, D.W., 2007, Convection and flow boiling in microgaps and porous foam coolers, Ph.D. dissertation, Dept. Mech. Eng., Univ. Maryland, College Park.

- Kuznetsov, V.V. and Shamirzaev, A.S., 2006, Boiling Heat Transfer for Freon R21 in Rectangular Minichannel,” Proceedings of the 4th International Conference on Nanochannels, Microchannels, and Minichannels, Limerick, Ireland, Paper No. ICNMM2006-96096.
- Lee, H.J. and Lee, S.Y., 2001, Heat Transfer Correlation for Boiling Flows in Small Rectangular Horizontal Channels with Low Aspect Ratios, *International Journal of Multiphase Flow*, Vol. 27, no. 12, pp. 2043-2062.
- Mandhane, J.M., Gregory, G.A., and Aziz, K., 1974, A Flow Pattern Map for Gas Liquid Flow in Horizontal Pipes, *International Journal of Multiphase Flow*, Vol. 1, no. 4, 537-553.
- Megahed, A., and Hassan, I., 2009. Two-Phase Pressure Drop and Flow Visualization of FC-72 in a Silicon Microchannel Heat Sink, *International Journal of Heat and fluid Flow*, 30, 1171 – 1182.
- Mikielewicz, D., Klugmann, M., and J. Wajs, 2012, Experimental Investigation of M-Shape Heat Transfer Coefficient Distribution of R123 Flow Boiling in Small-Diameter Tubes, *Heat Transfer Engineering*, 33(7):584–595, 2012
- Rahim, E., and Bar-Cohen, A., 2010. Parametric Dependence of Annular Flow Heat Transfer in Microgaps, Proceedings of the 14th International Heat Transfer Conference 2010, Washington, D.C., USA. Paper Number IHTC-23315.
- Rahim, E., Revellin, R., Thome, J.R., and Bar-Cohen, A., 2010, Characterization and Prediction of Two-Phase Flow Regimes in Miniature Tubes, *International Journal of Multiphase Flow*, 37, 12–23.
- Rahim, E., Bar-Cohen, A., and Ali, A., 2012, “Two-Phase Microgap Cooling of a Thermally-Simulated Microprocessor Chip,” Proceedings, IEEE ITherm Conference, San Diego, Ca.
- Revellin, R., 2005. Experimental two-phase fluid flow in microchannels, PhD Thesis (Prof. John R. Thome, Director), LTCM-EPFL, Swiss Federal Institute of Technology. <http://library.epfl.ch/theses/?nr=3437>
- Sheehan, J. R., Kim, D.H., and Bar-Cohen, A., 2009, “Thermal Imaging of Cooled Microgap Channel Wall”, *ASME/Pacific Rim Technical Conference and Exhibition on Packaging and Integration of Electronic and Photonic Systems, MEMS and NEMS*, IPACK2009-89238.
- Sheehan, J.R. and Bar-Cohen, A., 2010, “Spatial and Temporal Wall Temperature Fluctuations in Two-Phase Flow in Microgap Coolers”, *ASME International Mechanical Engineering Congress and Exposition*, IMECE2010-40227.
- Sheehan, J. R. and Bar-Cohen, A., 2011, “IR-Based Inverse calculation of two-phase Heat Transfer Coefficients in Microgap Channels ”, *ASME/Pacific Rim Technical Conference and Exhibition on Packaging and Integration of Electronic and Photonic Systems, MEMS and NEMS*, INTERPACK2011-52238.
- Shoham, O., 1982, Flow Pattern Transition and Characterization in Gas-Liquid Flow in Inclined Pipes, PhD. Dissertation, Tel-Aviv University, Ramat-Aviv, Israel.

Taitel, Y., and Dukler, A.E., 1976, A Model For Predicting Flow Regime Transitions in Horizontal and Near Horizontal Gas-Liquid Flow, *AIChE Journal*, Vol. 22, no. 1, pp. 47-55.

Taitel, Y., Lee, N., Dukler, A.E., 1978, Transient Gas-Liquid Flow in Horizontal Pipes: Modeling the Flow Pattern Transitions, *AIChE Journal*, Vol. 24, no. 5, pp. 920-934.

Taitel, Y., and Dukler, A.E., 1987, Effect of Pipe Length on the Transition Boundaries for High Viscosity Liquids, *International Journal of Multiphase Flow*, Vol. 13, no. 4, pp 577-581.

Taitel, Y., 1990, Flow Pattern Transition in Two Phase Flow, Keynote, Proc. of the 9th International Heat Transfer Conference, Jerusalem, Israel, pp. 237-254.

Yang, Y., and Fujita, Y., 2004, Flow Boiling Heat Transfer and Flow Pattern in Rectangular Channel of Mini-Gap, Proc. 2nd International Conference on Microchannels and Minichannels, New York, USA, Paper no. ICMM2004-2383.

Weisman, J., Duncan, D., Gibson, J., and Crawford, T., 1979, Effect of Fluid Properties and Pipe Diameter on Two-Phase Flow Pattern in Horizontal Lines, *International Journal of Multiphase Flow*, Vol. 5, no. 6, 437-462.